Design and performance of the Thomson scattering diagnostic on LHD

Design and performance of the Thomson scattering diagnostic on LHD

K. Narihara,[a] I. Yamada, H. Hayashi, and K. Yamauchi

National Institute for Fusion Science, Toki 502-5292, Japan

(Presented on 21 June 2000)

This article describes the design and performance of a multi-point (200) high repetition rate (4×50 Hz) Thomson scattering diagnostic installed on the Large Helical Device. A unique feature of this system is its oblique back scattering configuration, which enables us to observe the entire plasma region along a major radius on the midplane under a severely restricted port constraint. High throughput collection optics using a mosaic mirror of 1.5 m$\times$1.8 m area yield high quality data even with 0.5 J pulse energy delivered from 50 Hz repetition rate Nd: yttrium–aluminum–garnet lasers. High repetition and high spatial resolution (2–4 cm) of the system enable us to study island evolution in the plasma. © *2001 American Institute of Physics.* [DOI: 10.1063/1.1319368]

I. INTRODUCTION

The Thomson scattering (TS) diagnostic installed on the Large Helical Device (LHD) was put into operation in October 1998 after about seven years of design and construction activities.[1,2] It uses an oblique backscattering configuration, which enables us to observe the entire plasma region along a major radius on the midplane under a severely restricted port constraint. For this system to be viable, a slender laser beam over a long distance, a high pointing stability of laser beam, a large mosaic mirror, and an elaborated fiber optics were needed. Although we had an experience of designing and operating a TS system similar to the LHD TS on the Compact Helical System (CHS),[3] we worried about (a) the long term stability of the scattering configuration, (b) the attainable spatial resolution, (c) the throughput of the light collection optics, and (d) the stray light from the inner side of the vacuum chamber because the scattering angle, θ_{SCAT}, reaches nearer to 180°, due to the severe port constraint compared with the CHS case. In this article, we describe the actually observed performance of the LHD TS together with the design considerations and construction.

II. DESIGN AND CONSTRUCTION

The super conducting currents in a pair of helical coils and three pairs of poloidal coils generate a set of nested magnetic flux surfaces for plasma confinement as shown in Fig. 1. At the locations far from the magnetic axis the magnetic field lines become stochastic, forming a natural divertor. The magnetic axis shifts on the midplane ($z=0$ plane) as the plasma pressure increases or the vertical magnetic field is changed externally. Provided that electron temperature, T_e, and density, n_e, are constant on each magnetic surface, measurement along a major radius on the midplane is sufficient for obtaining T_e and n_e on the entire volume of plasma in any plasma state. Furthermore, the T_e and n_e profiles thus obtained will give the information on the shift and deformation of the nested magnetic surfaces. It is interesting

and important to study the plasma transport in the stochastic region as well as in the core region. From the above considerations, we chose to measure the entire region containing the nested flux surfaces and stochastic region, the region between A and B in Fig. 1. The production or enlargement of magnetic islands by plasma pressure in three-dimensional toroidal systems like LHD is a serious concern because of their detrimental effects on confinement. Considering the plasma crossing distance of 2 m at a horizontally elongated section, the spatial resolution ΔR less than 20 mm will be necessary for the island studies. Successive T_e and n_e profiles at transient phenomena induced, for example, by pellet injection, laser ablation, and pulse electron cyclotron heating will be valuable for studying the particle and heat transport. Considering the expected confinement time of 0.1–0.2 s, the repetition time much less than 0.1 s will be needed.

All these requirements in considerations, we made a comparison study among the then most advanced Thomson scattering systems, LIDAR (Joint European Torus),[4] TV-TS (Tokamak Fusion Test Reactor)[5] and YAG-TS (Axially Symmetric Divertor Experiment,[6] JIPP,[7] DIII-D[8]), and chose
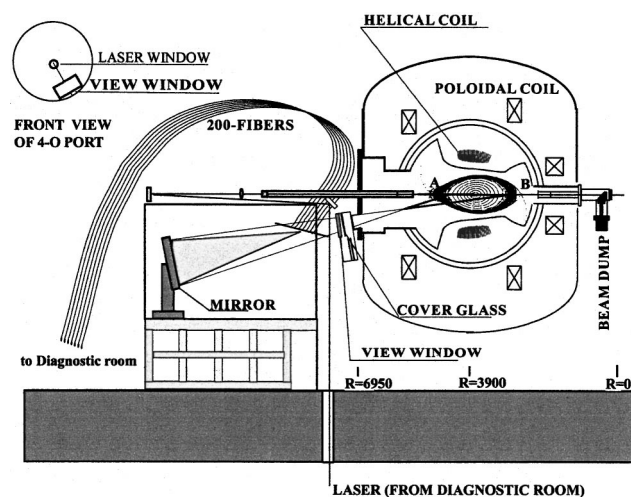

FIG. 1. A horizontally elongated section of LHD with Poincaré mapping of the magnetic field lines and the setup of the Thomson scattering diagnostic.

[a]Electronic mail: narihara@nifs.ac.jp

the YAG-TS as the LHD TS because it seemed to be most easily modified and improved to fulfill our requirements.

From the above argument, the laser beams pass through the center of the middle port (4-O) inwards. It was difficult to allocate a view window with sufficient size to see the entire laser beams in the plasma at right angle because of the presence of the helical coils wound around the vacuum chamber. The fact that the vacuum chamber is embedded in a Dewar, which keeps the super conducting coils at liquid helium temperature, inevitably makes the port length long. Under this severe port constraint, we examined the possibility of adopting a backscattering configuration like LIDAR in which the entire laser beam in plasma can be observed from a view window located close to the laser injection window. Contrary to the LIDAR case, the image of the laser beam should be resolved with $\Delta R \sim 20$ mm. Observing a laser beam with a diameter D_{LASER} from the direction designated by the angle θ_{SCAT} introduces a blur in the viewing position R_{SCAT} $\Delta R_{SCAT} = D_{LASER}/\tan(\theta_{SCAT})$, which diverges as θ_{SCAT} approaches $180°$. To realize the highest spatial resolution in the given port configuration while keeping a reasonable solid angle, we set a rectangular window of effective area of 35 cm$\times$60 cm at the farthest possible position from the central window through which the laser beam is injected. The scattered light passing through the view window should be collected and focused to form the image of the laser beam along which an array of fibers are placed. We compared a lens and a mirror for light collection optics. It is uncommon to use a mirror to form the image of an extended object. However, a mirror is very attractive for the present purpose in that it is very strong to neutron radiation from the plasma, that it is free from color aberration and that the size can be extended easily with a reasonable cost. Examining the image of the laser beam formed by a mirror with various radii of curvature located at various positions, we found that the image quality is best when the center of curvature locates at the center of the window. This is because, in this configuration, every light ray passes near the center of the sphere, reducing all aberrations except the spherical one. The diameter of the circle of the least confusion for spherical aberration is calculated as

$$D_{DCLC} = (R_c/32)(D_c/R_c)^3 (1-m)^2/(1+m),$$

where m is the magnification, R_c is the radius of curvature, and D_c is the diameter (effective diagonal) of the mirror. Requiring that D_{DCLC}, which is a smoothly decreasing function of R_c, be less than the image size, we chose the minimum permissible $R_c = 4.5$ m and the width of the mirror$=1.5$ m to match the window size. It should be noted that the portion of the mirror surface used is different for different scattering position; the outer (inner) scattering position uses the lower (higher) portion of the mirror surface. This is the reason why the mirror size is as large as 1.5 m$\times$1.8 m and the image quality is kept above a permissible level. The backscattering configuration thus chosen is depicted in Fig. 1. The backscattering angle, $\theta_{BACK} = 180° - \theta_{SCAT}$, the incidence angle at the fiber's surface θ_{INC}, the magnification m, solid angle $\Delta\Omega$, diameter of the least confusion circle D_{DCLC}, the diameter of the laser beam D_{LASER}, the diameter
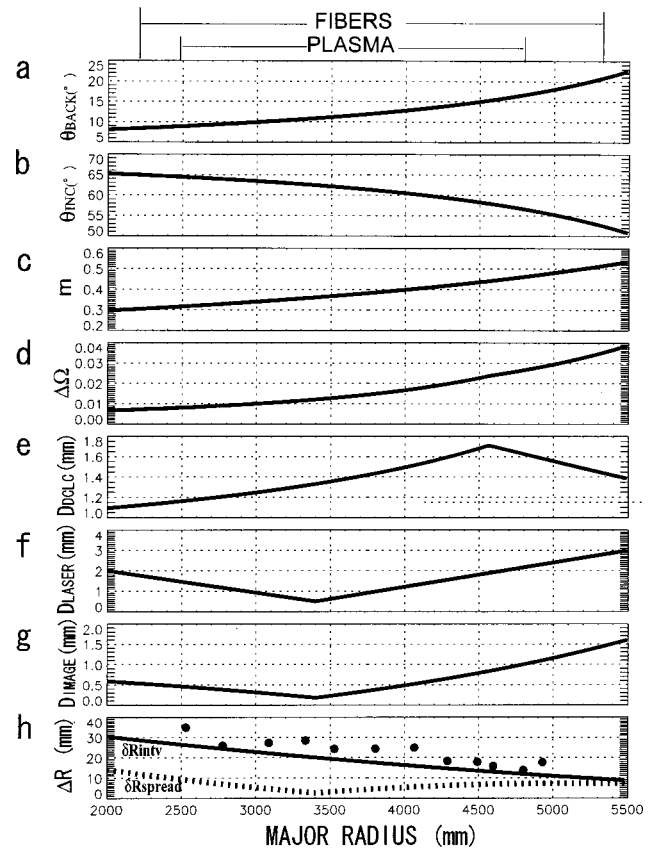

FIG. 2. Scattering position R_{SCAT} dependencies of (a) backscattering angle ($180°$ scattering angle), (b) incidence angle at the fiber's surface, (c) magnification, (d) solid angle, (e) diameter of circle of the least confusion, (f) diameter of the laser beam, (g) diameter of the laser's image, (h) spatial resolution. The symbol ● denotes the measured widths ΔR_{obs}.

of the laser's image D_{IMAGE}, spatial resolution ΔR are shown in Fig. 2 as a function of the scattering position R_{SCAT}. A single mirror of the above mentioned shape and size is very heavy and expensive to construct. To alleviate these difficulties, we constructed a mosaic mirror composed of 132 hexagonal mirrors with 87 mm side length. The hexagonal mirrors were set on a skeleton structure made of fiber reinforced plastic with screws. The position and angular orientation of each mirror was adjusted so that the image of a tiny light source (0.1-mm-diam fiber) formed by each small mirror be minimized and coincide with a fiducial point on a charge coupled device (CCD) plate. The image quality of the mosaic mirror could be improved appreciably compared with a single large mirror by adjusting the orientation of the peripheral mirrors. The heavily oblique scattering configuration requires the laser beam have a small diameter over a long distance (2.5 m) and also its position be highly stable to realize a high spatial resolution. The laser beams travel ~ 50 m from a laser set in the diagnostic room to the beam dump set inside the inner middle port (4-I) by use of five steering mirrors. The beam diameter of 9 mm at the laser exit grows as it travels to 15 mm at an $f = 9$ m focusing lens set near the laser injection window and then reduces to the minimum of 1.5 mm at $R = 3.4$ m. The beam diameter as a function of the scattering position is shown in Fig. 2(f) together with its
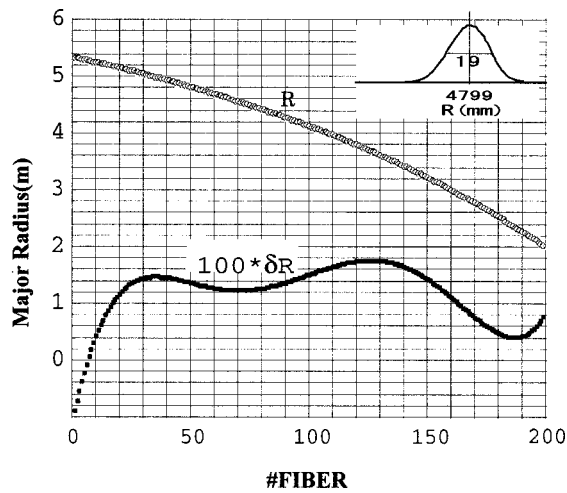
FIG. 3. Scattering position R_{SCAT} as a function of the fiber channel. The change of this relation over a half year is over plotted. In inset is the light signal from 51 fiber as a function of the target position.

FIG. 4. Raw data at $R_{SCAT}=2788$ mm.

corresponding image diameter, Fig. 2(g). The specified pointing stability of the laser (NY80-50 Continuum, pulse energy 0.55 J, pulse width 10 ns, beam diameter 9 mm) is 0.4 mr, which would introduce the transverse variation of the beam position at $R_{SCAT}=4.9$ m (1.5 m from the waist) $\delta=0.4$ mr* 50 m* 1.5 m/7 m=4.3 mm, which is beyond the fiber's scope. We solved this difficulty by correcting the tilt of the first steering mirror so that the beam position of the previous laser shot, monitored at 10 m ahead from the laser, is in an allowed distance from a reference point.[9] Although the beam direction randomly walks with a time constant of seconds, the correlation between the beam directions of the successive laser shots is very high, validating the above feedback control with ~100 times reduction of the random walk amplitude. The repetition rate of a laser with an output energy of an order of 1 J is limited to ~50 Hz by the thermal effects on the laser components. In order to raise the repetition rate, we adopted the ''beam packing'' method first developed on Doublet-III.[7] The mirror system[3] we developed can pack up to seven laser beams into a circle of 42 mm in diameter, of which we actually packed four lasers.

It is possible only by the use of fibers to dissect the heavily inclined image of the laser beam and then to transport the collected light to the polychromators set in the diagnostic room. The larger diameter of the fiber would relax the requirement for the image forming optics, but would result in the worse spatial resolution and higher fabrication cost. We chose a single fiber of 2 mm in diameter and numerical aperture of 0.25. The tips of the arrayed fibers were cut at 55° to avoid the blocking due to the otherwise neighboring fibers.[3] The fiber to fiber distance on the laser image is 2.93 mm, giving the separation between successive scattering volumes δR_{intv} as shown in Fig. 2(h). The finite size of the laser beam brings in to the image blur δR_{SPREAD}. The light scattered at a volume and passing the center of the window is incident to a fiber end surface with the incident angle θ_{INC} shown in Fig. 2(b). These large incident angles imply that the transmission at the fiber tip is heavily dependent on the polarization of the incident light, which necessitates the po-
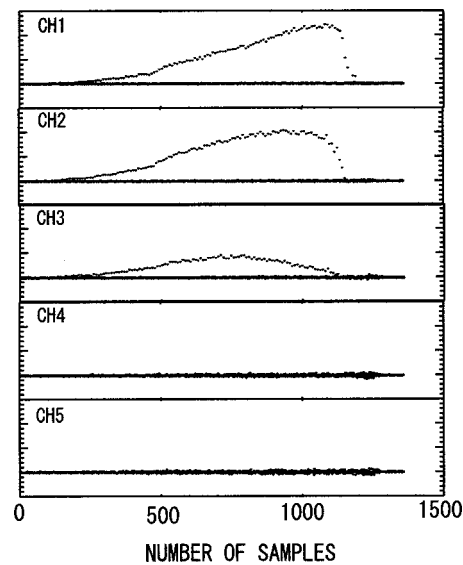
larization of the laser beam be adjusted. Because θ_{INC} is close to Brewster's angle (~55°), the efficiency of the scattered light being transmitted and transported in the fibers is higher than 98% for all fibers. In the planned deuterium neutral beam injection (NBI) experiment, a neutron flux of ~10^{11} n/cm^2/shot is expected to expose the ends of fibers. This radiation would induce wavelength dependent transmission loss, thus causing systematic errors in the deduced electron temperature and density. Fibers containing rich OH have high resistance to radiation, but they have high attenuation around $\lambda=950$ nm, and therefore cannot be used for our purpose. We have had developed pure silica fiber that has good radiation resistance in the wavelength region 700 nm $<\lambda<1200$ nm. When the fiber was exposed to 1 MR Co-60 source, the transmission loss increased by 8 dB/km at $\lambda=800$ nm and 2 dB/km at $\lambda=1000$ nm.

The view window of the effective area of 35 cm×60 cm was made of fused quartz of 40 cm×66 cm×5 cm, which works both to seal the vacuum and to transmit the scattered light. The expected heat load to the window is ~10 W/cm^2 at the maximum power of NBI. Soft x-ray and neutral particles, dominant heat carriers, deposit in a very thin region at the front surface of the window, inducing large stress on the surface. To avoid damage of the view window, we adopt a two-glass scheme as shown in Fig. 1, in which the first 1.5-cm-thick glass (cover glass) catches the heat and the second 5-cm-thick window withstands the vacuum pressure. If the cover glass is darkened by sputtered impurity accumulation, it is replaced with a backup set below. Three replacements are possible without breaking vacuum.

A beam dump made of carbon block backed by an S304 plate, which is retractable from the laser beam path for beam alignment purpose, is set at the end of a 1.5-m-long laser guide tube with stacked baffles.

Five-filter polychromators similar to that installed on DIIID[5] were fabricated. All the optical and electrical components are housed in an aluminum case of 455×200×53 mm^3. To stabilize the gain of the avalanche photodiodes, the tem-
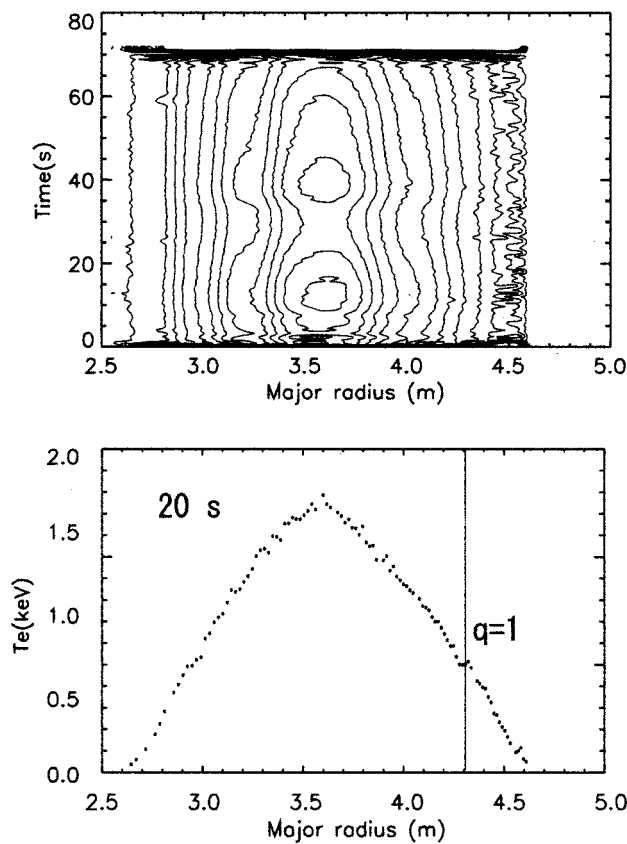
FIG. 5. An example of T_e profile of a long pulse plasma. A flattening in T_e probably due to an island is noticed at $R_{SCAT} \sim 4340$ mm. The data are the average of five laser shots.

perature of the cases is regulated by a water flow.

The number of signals per event are 5×200 scattering plus 24 monitor signals including laser power, timing of the laser fire, and the lateral laser beam positions at several locations on the laser beam path. These signals are analog-to-digital converted by charge ADCs (Lecroy 1881M FAST-BUS). We chose this ADC because of its short conversion time (12 μs), high density (64 channels per slot), high resolution, and wide dynamic range (13 bit). In addition to the scattering events, eight background events are acquired every 20 μs after every laser shot to estimate the variance of the signals.

III. PERFORMANCE

The scattering position R_{SCAT} and spatial resolution were measured by sweeping the position of a target illuminated by a HeNe laser while the scattered light was measured on each fiber. The path and beam size of the HeNe was carefully adjusted to coincide with those of the central Nd:YAG laser beam, which was valid since the mirror produces no chromatic abberation. As an example, the signal from 51 fiber is shown in an inset in Fig. 3. We define R_{SCAT} by the position where the signal peaks, and the spatial resolution ΔR_{obs} as the full width at half maximum. The R_{SCAT} as a function of

the fiber channel is shown in Fig. 3. This relation is very sensitive to the variation of the beam-mirror-fiber configuration for the heavily oblique backscattering configuration as employed here. The change of the scattering position over a half year is over plotted. The maximum change of 18 mm is still large for precise profile studies. Although four laser beams are tightly packed, the heavily oblique scattering configuration inevitably introduces appreciable differences in the scattering position for different lasers, requiring us to discriminate the lasers used for every laser shot.

The image quality of a tiny light source (0.1 mm in diameter) placed near the center of the mosaic mirror's curvature was occasionally monitored on a CCD plate. Although the spot size gradually grows, the light collecting efficiency seems to be practically unchanged for a year after a fine adjustment of the orientations of the small mirrors.

The stray laser light appearing on the signals is a serious concern. The inner channels are most likely to catch stray light due to the proximity to the laser exit tube in the viewing scope. The raw data of a channel ($R = 2.788$ m) is shown in Fig. 4. Stray light would appear even in the absence of plasma. No such signal can be noticed.

A contour plot and a snap shot of T_e (R_{SCAT}, t) of a long pulse plasma are shown in Fig. 5. The plasma fills the volume enclosed by magnetic surfaces and extends further $\sim$10 cm from the last closed surface. This region is covered by $\sim$110 fibers' scope. On the other fibers that view the stochastic field region, no appreciable signals appear with the present laser energy. We can notice a flat region in T_e around $R \sim 4.3$ m, where $q \sim 1$, caused by an $m/n = 1/1$ island generated by an error field. This error field island reduces its size appreciably in the presence of plasma.

We tried absolute sensitivity calibrations based on Raman scattering several times, but the results were not reproducible. We speculate that this is due to the smallness of Raman signals and the incomplete beam pointing stability. This is one of the important unsettled problems.

[1] K. Narihara, K. Yamauchi, I. Yamada, T. Minami, K. Adachi, A. Ejiri, Y. Hamada, K. Ida, H. Iguchi, K. Kawahata, T. Ozaki, and K. Toi, Fusion Eng. Des. **34-35**, 67 (1997).
[2] M. Fujiwara *et al.*, J. Fusion Energy **15**, 125 (1996).
[3] K. Narihara, T. Minami, I. Yamada, and K. Yamauchi, Rev. Sci. Instrum. **66**, 4607 (1995).
[4] H. Salzmann, J. Bundgaard, A. Gadd, C. Gowers, K. B. Hansen, K. Hirsch, P. Nielsen, K. Reed, C. Schrödter, and K. Weisberg, Rev. Sci. Instrum. **59**, 1451 (1988).
[5] D. Johnson, N. Bretz, D. Dimock, B. Grek, D. Long, R. Palladino, and E. Tolnas, Rev. Sci. Instrum. **57**, 1856 (1986).
[6] H. Rohr, K.-H. Steuer, G. Schramm, K. Hirsch, and H. Salzmann, Nucl. Fusion **22**, 1099 (1982).
[7] K. Narihara, K. Yamauchi, T. Minami, I. Yamada, K. Sato, K. Kawahata, Y. Hamada, M. Kojima, and S. Hirokura, Jpn. J. Appl. Phys. **35**, 266 (1996).
[8] T. N. Carlstrom, G. L. Campbell, L. C. DeBoo, R. Evanko, J. Evans, C. M. Greenfield, J. Haskovec, C. L. Hsieh, E. McKee, R. T. Snider, R. Stockdale, P. K. Trost, and M. P. Thomas, Rev. Sci. Instrum. **63**, 4901 (1992).
[9] I. Yamada, K. Narihara, K. Yamauchi, and H. Hayashi, Rev. Sci. Instrum., these proceedings.